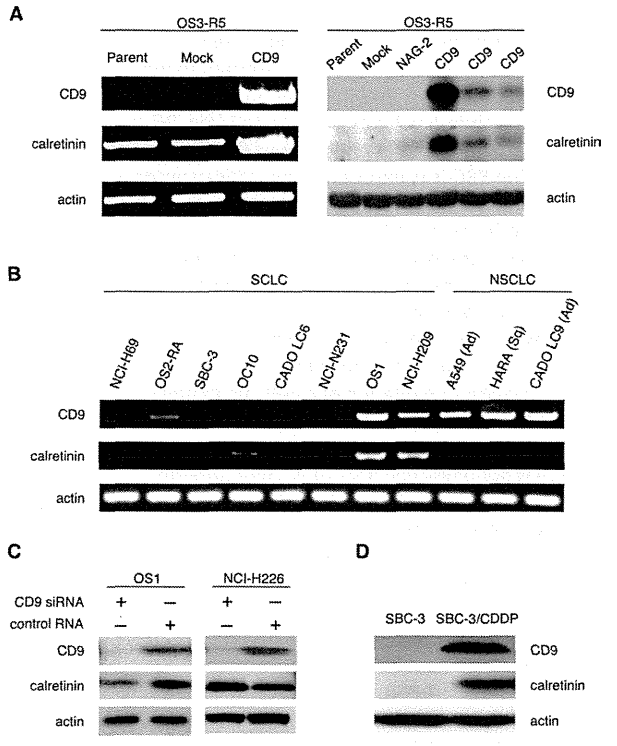

Fig. 2. Co-expression of CD9 and calretinin in SCLC cells. (A) Total RNA was extracted from the parent, mock transfectant, and CD9 transfectant of OS3-R5 and analyzed for expressions of CD9 and calretinin by RT-PCR. β-Actin amplification was used as the internal control (*left*). The parent, mock transfectant, NAG-2 transfectant, and CD9 transfectants of OS3-R5 were lysed with 1% Brij 99 lysis buffer. Cell lysates were analyzed for expressions of CD9 and calretinin by immunoblotting. Anti-β-actin blots were used as the internal control (*right*). (B) Total RNA was extracted from multiple SCLC and NSCLC cell lines and analyzed for expressions of CD9 and calretinin by RT-PCR. Ad, adenocarcinoma; Sq, squamous cell carcinoma. (C) An SCLC line OS1 (*left*) or a mesothelioma line NCI-H226 (*right*) was transfected with siRNAs against CD9 or control RNAs. Cell lysates were analyzed for expressions of CD9 and calretinin by immunoblotting. (D) Cell lysates of SCLC lines SBC-3 and SBC-3/CDDP were analyzed for expressions of CD9 and calretinin by immunoblotting.

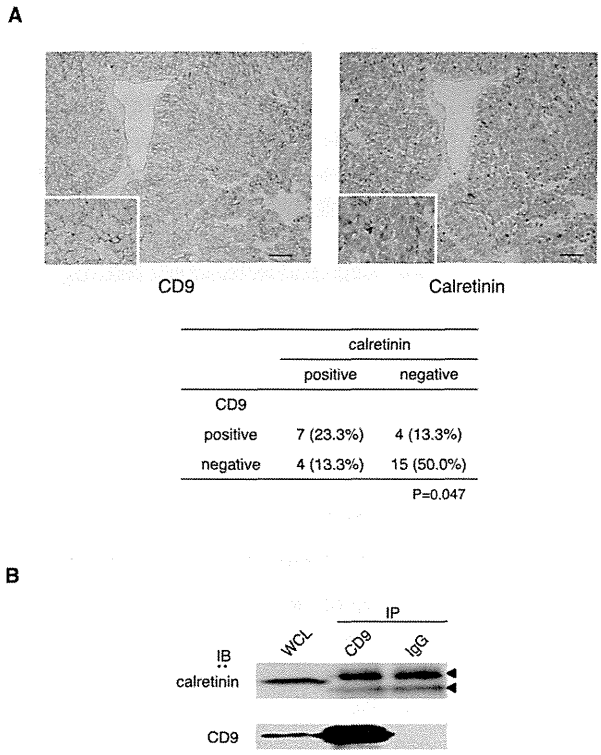

	calretinin	
	positive	negative
CD9		
positive	7 (23.3%)	4 (13.3%)
negative	4 (13.3%)	15 (50.0%)

P=0.047

Fig. 3. CD9 is not physically associated with calretinin. (A) Immunohistochemical staining of CD9 and calretinin in a double-positive specimen from an SCLC tissue microarray. *Insets* show enlarged images of a part of sections. Bar, 50 μm. Significant association between CD9 and calretinin expressions in the tissue microarray was evaluated by Fisher's exact test (*table*). (B) CD9 and calretinin in whole cell lysate (WCL) and in immunoprecipitates (IP) with anti-CD9 mAb or control IgG of OS3-R5-CD9 were immunoblotted (IB). *Arrowheads* indicate nonspecific binding of secondary Abs.

2.10. Mice

The generation of CD9 knockout (KO) mice was described previously [13]. These mice were backcrossed more than six generations into the C57BL/6J background. The mice were bred in a barrier facility, and all animal procedures were performed in accordance with the Osaka University guidelines on animal care.

2.11. Apoptosis analysis

Cells were transfected with siRNA against calretinin or negative control RNAs. After 24 h, the cells were cultured in the absence or presence of CDDP in low-serum (0.1% FBS) RPMI 1640 for 48 h. Apoptotic cleavage of PARP [14] and decrease of Akt phosphorylation [9] were analyzed by immunoblotting. Viable cells were quantified with Cell Counting Kit-8 (Dojindo Laboratories, Kumamoto, Japan). Assays were performed in triplicate cultures and values are expressed as mean ± SD. Statistical differences were determined by Student's *t*-test. $P < 0.05$ was considered statistically significant.

3. Results

3.1. Identification of proteins upregulated in OS3-R5-CD9 cells

We previously established a CD9 (−) SCLC cell line OS3-R5 and its CD9 transfectant OS3-R5-CD9 and revealed that the CD9 transfectants were less motile on fibronectin [8] and revealed enhanced apoptosis in low-serum culture conditions [9]. To detect molecules that regulate these changes, cell lysates of the parent, mock transfectant, and CD9 transfectant of OS3-R5 (Fig. 1A) were subjected to 2-DE, and protein spots were visualized by silver stain of the gels. Spots selectively overexpressed in OS3-R5-CD9 were identified (Fig. 1B) and the corresponding proteins were analyzed by mass spectrometry. We repeated this experiment and found that two proteins, a calcium-binding protein, calretinin, and a proteasome activator subunit 1, PA28α, were reproducibly overexpressed in OS3-R5-CD9 cells (Table S1). Fig. 1C shows PMF spectra of spot 2 obtained by MALDI-TOF. Matched peptides were found to cover 33% of protein sequence of calretinin (Fig. 1D). Based on the fact that SCLC has neuronal features, we further analyzed calretinin, which is a protein distributed in the nervous system.

3.2. Co-expression of CD9 and calretinin in SCLC cells

RT-PCR revealed that the calretinin gene was minimally transcribed in the parent and mock-transfected OS3-R5 cells, and that ectopic expression of CD9 promoted its transcription (Fig. 2A, *left column*). To test the calretinin induction is specifically related to CD9, multiple CD9 transfectants and cells transfected with another tetraspanin NAG-2 were examined. As shown in Fig. 2A, *right column*,

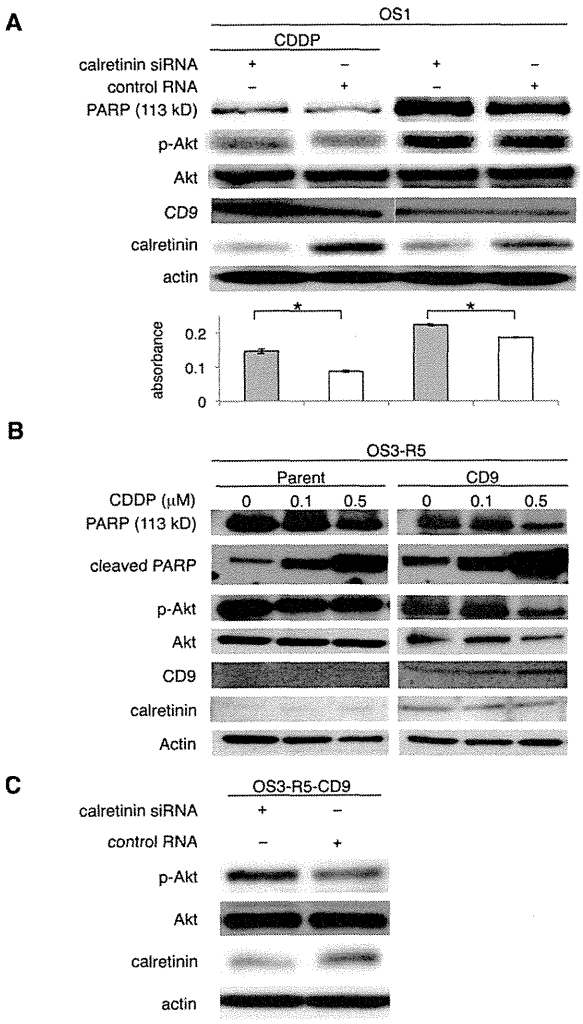

Fig. 4. *Calretinin promotes apoptosis of CD9 (+) SCLC cells.* (A) CD9 (+)/calretinin (+) OS1 cells were transfected with siRNAs against calretinin or control RNAs and cultured in low-serum conditions in the absence or presence of 5 μM CDDP for 48 h. Cell lysates were analyzed for expressions of PARP (113 kD), phosphorylated Akt (p-Akt), total Akt, CD9, and calretinin by immunoblotting. Anti-β-actin blots were used as the internal control (*upper*). Viable cells were quantified with a cell counting kit (*lower*). *$P < 0.01$. (B) The parent and CD9 transfectant of OS3-R5 were cultured in low-serum conditions in the indicated concentrations of CDDP for 48 h. Cell lysates were analyzed for expressions of PARP (113 kD), cleaved PARP, phosphorylated Akt, total Akt, CD9, and calretinin by immunoblotting. (C) OS3-R5-CD9 cells were transfected with siRNAs against calretinin or control RNAs and cultured in low-serum conditions for 48 h. Cell lysates were analyzed for expressions of phosphorylated Akt, total Akt, and calretinin by immunoblotting.

calretinin was almost absent in the parent, mock transfectant, and NAG-2 transfectant in immunoblotting, whereas calretinin was obviously present in three independent CD9 transfectants and its level was parallel to that of CD9. We further examined if CD9 and calretinin are co-expressed in a panel of lung tumor cell line (Fig. 2B). Consistent with our previous report that most SCLC cells lack CD9 [8], five of eight SCLC lines revealed no transcription and one cell line (OS2-RA) showed only marginal transcription of *CD9* gene. The other two lines (OS1 and NCI-H209) clearly expressed CD9, and these CD9 (+) lines also expressed calretinin. Meanwhile, all three NSCLC lines were CD9 (+), but none of them expressed calretinin (Fig. 2B).

CD9 was next deleted by knockdown with siRNA in the SCLC line OS1, which expresses endogenous CD9. As shown in Fig. 2C, *left column*, the knockdown of CD9 suppressed the level of calretinin. In an additional experiment, we have studied CD9 and calretinin expressions in multiple pleural mesothelioma cell lines and found that only NCI-H226 expresses both CD9 and calretinin in immunoblotting (Fig. S1). CD9 was knocked down in this mesothelioma line, but unlike OS1, the calretinin level was not affected (Fig. 2C, *right column*). Our recent report showed that endogenous CD9 is induced when the CD9 (−) SCLC line SBC-3 is exposed to an anticancer drug, cisplatin [10]. As shown in Fig. 2D, calretinin was co-induced with endogenous CD9 in the cisplatin-exposed SBC-3 cells.

We further investigated if CD9 is generally required for the expression of calretinin using tissues from wild-type and CD9 KO mice. Calretinin was expressed in liver and brain lysates of wild-type mice, and its levels were not affected by the loss of CD9, as evidenced by abundant expression of calretinin in the lysates from CD9 KO mice (Fig. S2). Together, regulation of calretinin expression by CD9 seemed to be specific to human SCLC cells.

3.3. *CD9 is not physically associated with calretinin*

To investigate co-expressions of CD9 and calretinin *in vivo*, a tissue microarray of SCLC was analyzed by immunohistochemistry. Among 30 patients, 11 were CD9 (+), 11 were calretinin (+), and 7 were double-positive, and association between CD9 expression and calretinin expression was weakly significant (Fig. 3A, *table*). Higher positive rate of CD9 (11/30) in SCLC tissues compared with that in SCLC cell lines [8] might be because some biopsy specimens were obtained from relapsed or metastatic lesions, which were more frequently CD9 (+) than pretreated primary tumors [10]. Representative staining of CD9 and calretinin in a double-positive specimen indicated that expression patterns of these proteins were different (Fig. 3A). CD9 was stained at the cell periphery, whereas calretinin showed nuclear and cytoplasmic staining (Fig. 3A, *insets*). Tetraspanins including CD9 are characterized by their propensity to form multiprotein complexes at the plasma membrane. To examine if calretinin is present in large protein complexes including CD9, co-precipitated proteins with CD9 was immunoblotted with anti-calretinin Ab. As shown in Fig. 3B, calretinin did not co-precipitate with CD9 in OS3-R5-CD9 cell lysate even using non-stringent detergent, Brij 99. Thus, calretinin was not present in the protein complex including CD9.

3.4. *Calretinin promotes apoptosis of CD9 (+) SCLC cells*

Our previous reports have shown that ectopic expression of CD9 increases apoptosis by attenuation of postadhesive phosphorylation of Akt [9] and that anticancer drugs induce endogenous CD9 in SCLC cell lines [10]. To examine the involvement of calretinin in apoptosis of SCLC cells, calretinin was knocked down with siRNA in CD9 (+)/calretinin (+) OS1 cells, and expression of PARP was examined as an indicator of apoptotic cell death [14]. Exposure of OS1 cells to 5 μM cisplatin increased endogenous CD9 and calretinin and enhanced apoptosis as evidenced by decrease of 113-kD PARP and decreased phosphorylation of Akt (Fig. 4A, control RNA). Knockdown of calretinin prevented the OS1 apoptosis regardless of the exposure to cisplatin (Fig. 4A, calretinin siRNA). It appeared that the calretinin knockdown slightly upregulated CD9; this might reflect an unknown feedback mechanism. Proapoptotic role of calretinin was also studied in OS3-R5 cells. The exposure to CDDP for only 48 h did not induce endogenous CD9 and calretinin in this cell line and, when compared with the parent cells, OS3-R5-CD9 cells expressing calretinin revealed higher sensitivity to CDDP, as evidenced by enhanced PARP cleavage and decreased Akt phosphorylation (Fig. 4B). After the exposure to 1 μM CDDP for 48 h, viable cells of OS3-R5 and OS3-R5-CD9 were 56.1 ± 1.8% and 20.1 ± 2.7%, respectively ($P < 0.01$). As shown in Fig. 4C, the knockdown of calretinin in OS3-R5-CD9 increased phosphorylation of Akt. These results suggest that calretinin may be a downstream mediator of apoptosis in CD9 (+) SCLC cells.

4. Discussion

Our previous studies have proposed that the absence of tetraspanin CD9 contributes to highly malignant phenotype of SCLC and that CD9 may be a pivotal regulator of SCLC cell survival [8–10]. In the present study using a proteomics-based approach, we identified calretinin as a possible mediator of CD9-induced apoptosis in SCLC. Calretinin was present in CD9 (+) SCLC cell lines but not in CD9 (−) SCLC lines and CD9 (+) NSCLC lines. Ectopic or CDDP-induced expression of CD9 upregulated calretinin in SCLC lines. Knockdown of CD9 conversely down-regulated calretinin in an SCLC line but not in a mesothelima cell line. Furthermore, knockdown of calretinin increased Akt phosphorylation and decreased apoptosis in CD9 (+)/calretinin (+) SCLC cell lines. Although statistical significance in the association of CD9 and calretinin expressions was weak ($P = 0.047$) in SCLC tissues, we speculate that this might be due to elimination of apoptotic CD9 (+)/calretinin (+) tumor cells *in vivo*.

Calretinin is a member of the calcium-binding protein EF-hand family first identified in the retina. Calcium-binding proteins including calretinin are expressed in neuronal subpopulations of the nervous system. Calretinin is involved in cellular functions including intracellular calcium buffering, messenger targeting, and the modulation of neuronal excitability. Modulation of calcium signaling by calretinin is important for timing and plasticity of synaptic events in neuronal networks. Some studies have suggested neuroprotective role of calretinin against calcium-induced cytotoxicity, whereas others reported opposite effects [15,16]. Of note, a recent report using colorectal cancer cells indicated that calretinin is induced following treatment with oxaliplatin or 5-FU and positively regulates apoptotic signals via as yet unknown mechanisms [14]. In line with this report, the present study suggested that calretinin mediates proapoptotic signaling in SCLC cells and for the first time showed that CD9 positively regulates the expression of calretinin. It has been established that tetraspanins including CD9 work as organizer of multiprotein complexes at the membrane [4,5]. Although calretinin has been reported to concentrate beneath the plasma membrane during maturation in neurons [17], it did not co-precipitate with CD9 in OS3-R5-CD9 cells, suggesting the presence of other mediators linking CD9 to enhanced expression of calretinin.

In conclusion, by proteomics-based approach, we have proposed a novel proapoptotic pathway that links the metastatic suppressor CD9 to the neuronal calcium-binding protein, calretinin, in SCLC. Induction of CD9/calretinin may at least partially account for its high sensitivity to chemotherapy and might provide clues to new therapeutic approach to suppress early growth, metastasis, and recurrence of SCLC.

Acknowledgments

We thank Y. Habe for secretarial assistance. This work was supported in part by a Grant-in-Aid for Scientific Research from the Ministry of Education, Culture, Sports, Science and Technology and a Health and Labour Sciences Research Grant from the Ministry of Health, Labour and Welfare, Japan.

Supplementary material

Supplementary material associated with this article can be found, in the online version, at doi:10.1016/j.fob.2013.04.005.

References

[1] Stovold R., Blackhall F., Meredith S., Hou J., Dive C., White A. (2012) Biomarkers for small cell lung cancer: neuroendocrine, epithelial and circulating tumour cells. Lung Cancer 76, 263–268.
[2] Califano R., Abidin A.Z., Peck R., Faivre-Finn C., Lorigan P. (2012) Management of small cell lung cancer: recent developments for optimal care. Drugs 72, 471–490.
[3] Kitamura H., Yazawa T., Sato H., Okudela K., Shimoyamada H. (2009) Small cell lung cancer: significance of RB alterations and TTF-1 expression in its carcinogenesis, phenotype, and biology. Endocr. Pathol. 20, 101–107.
[4] Charrin S., le Naour F., Silvie O., Milhiet P.E., Boucheix C., Rubinstein E. (2009) Lateral organization of membrane proteins: tetraspanins spin their web. Biochem. J. 420, 133–154.
[5] Yanez-Mo M., Barreiro O., Gordon-Alonso M., Sala-Valdes M., Sanchez-Madrid F. (2009) Tetraspanin-enriched microdomains: a functional unit in cell plasma membranes. Trends Cell. Biol. 19, 434–446.
[6] Malik F.A., Sanders A.J., Jiang W.G. (2009) KAI-1/CD82, the molecule and clinical implication in cancer and cancer metastasis. Histol. Histopathol. 24, 519–530.
[7] Wang H.X., Li Q., Sharma C., Knoblich K., Hemler M.E. (2011) Tetraspanin protein contributions to cancer. Biochem. Soc. Trans. 39, 547–552.
[8] Funakoshi T., Tachibana I., Hoshida Y., Kimura H., Takeda Y., Kijima T. et al. (2003) Expression of tetraspanins in human lung cancer cells: frequent downregulation of CD9 and its contribution to cell motility in small cell lung cancer. Oncogene 22, 674–687.
[9] Saito Y., Tachibana I., Takeda Y., Yamane H., He P., Suzuki M. et al. (2006) Absence of CD9 enhances adhesion-dependent morphologic differentiation, survival, and matrix metalloproteinase-2 production in small cell lung cancer cells. Cancer Res. 66, 9557–9565.
[10] Kohmo S., Kijima T., Otani Y., Mori M., Minami T., Takahashi R. et al. (2010) Cell surface tetraspanin CD9 mediates chemoresistance in small cell lung cancer. Cancer Res. 70, 8025–8035.
[11] Kumagai T., Tanio Y., Osaki T., Hosoe S., Tachibana I., Ueno K. et al. (1996) Eradication of Myc-overexpressing small cell lung cancer cells transfected with herpes simplex virus thymidine kinase gene containing Myc-Max response elements. Cancer Res. 56, 354–358.
[12] Shevchenko A., Wilm M., Vorm O., Mann M. (1996) Mass spectrometric sequencing of proteins silver-stained polyacrylamide gels. Anal. Chem. 68, 850–858.
[13] Yamane H., Tachibana I., Takeda Y., Saito Y., Tamura Y., He P. et al. (2005) Propionibacterium acnes-induced hepatic granuloma formation is impaired in mice lacking tetraspanin CD9. J. Pathol. 206, 486–492.
[14] Boyer J., Allen W.L., McLean E.G., Wilson P.M., McCulla A., Moore S. et al. (2006) Pharmacogenomic identification of novel determinants of response to chemotherapy in colon cancer. Cancer Res. 66, 2765–2777.
[15] Camp A.J., Wijesinghe R. (2009) Calretinin: modulator of neuronal excitability. Int. J. Biochem. Cell Biol. 41, 2118–2121.
[16] Barinka F., Druga R. (2010) Calretinin expression in the mammalian neocortex: a review. Physiol. Res. 59, 665–677.
[17] Hack N.J., Wride M.C., Charters K.M., Kater S.B., Parks T.N. (2000) Developmental changes in the subcellular localization of calretinin. J. Neurosci. 20, RC67.

Jpn J Radiol (2013) 31:677–684
DOI 10.1007/s11604-013-0235-3

ORIGINAL ARTICLE

Computer-assisted solid lung nodule 3D volumetry on CT: influence of scan mode and iterative reconstruction: a CT phantom study

Adriaan Coenen · Osamu Honda · Eric J. van der Jagt · Noriyuki Tomiyama

Received: 27 May 2013 / Accepted: 31 July 2013 / Published online: 18 August 2013

Abstract
Objective To evaluate the effect of high-resolution scan mode and iterative reconstruction on lung nodule 3D volumetry.
Methods Solid nodules with various sizes (5, 8, 10 and 12 mm) were placed inside a chest phantom. CT images were obtained with various tube currents, scan modes (conventional mode, high-resolution mode) and iterative reconstructions [0, 50 and 100 % blending of adaptive statistical iterative reconstruction (ASiR) and filtered back projection]. The nodule volumes were calculated using semiautomatic software and compared with the assumed volume from the nodules.
Results The mean absolute and relative percentage error improved when using iterative reconstruction especially when using the conventional scan mode; however, this effect was not significant. Significant reduction in volume overestimation was observed when using high-resolution scan mode ($P = 0.011$).
Conclusion The high-resolution mode significantly reduces the volume overestimation of 3D volumetry. Iterative reconstruction shows a reduction in volume overestimation and error margin especially with the conventional scan mode; however, this effect was not significant.

Keywords Pulmonary nodule · 3D volumetry · Phantom · Iterative reconstruction · High-resolution mode · ASiR

A. Coenen · O. Honda · N. Tomiyama
Department of Radiology, Osaka University Graduate School of Medicine, 2-2 Yamadaoka, Suita City, Osaka 565-0871, Japan

A. Coenen
Faculty of Medical Sciences, University of Groningen, Antonius Deusinglaan 1, 9713 AV Groningen, The Netherlands

A. Coenen (✉)
Erasmus MC (Hospital), s-Gravendijkwal 230, 3015 CE Rotterdam, The Netherlands
e-mail: adriaancoenen@gmail.com

E. J. van der Jagt
Department of Radiology, University Medical Center Groningen, Hanzeplein 1, 9713 GZ Groningen, The Netherlands

Introduction

Lung cancer is the most commonly diagnosed form of cancer, with a worldwide incidence of 1.2 million and a mortality of approximately 1.1 million [1]. Early stage lung cancer most commonly presents as a small pulmonary nodule on a CT scan. If the nodule is suspect for malignancy, further evaluation with positron emission tomography (PET) or follow-up with a CT scan is advised. The follow-up CT scan can be used to determine possible nodule growth.

It is reported that the majority of malignant nodules double in volume in 20–400 days [2]. A study by Ashraf et al. [3] shows that volume growth of small lung nodules is associated with lung cancer. This association emphasises the need for reliable volume measurements used to calculated volume growth. Currently, growth of pulmonary nodules is measured using the largest diameters on transverse cross-sectional slices in daily clinical work [4].

Currently, computer-aided 3D volumetry of pulmonary nodules is not used in the daily clinical setting. But it is recognised that computer-aided 3D volumetry has better reliability and reproducibility compared to manual assessment with small interobserver variance. It is also

recognised that some scan or reconstruction parameters affect computer-aided 3D volumetry [5]. Previously studies have investigated the effects of scan and reconstruction parameters such as the tube current, reconstruction kernel and field of view [6, 7].

Recent CT techniques can produce better CT images with a higher spatial resolution and lower image noise. In this study we evaluated the effect of a high-resolution scan mode and iterative reconstruction on 3D volumetry. High-resolution mode is a technique based on garnet detectors. It is capable of an increased number of views per gantry rotation, allowing for an increase in sampling. This increased amount of sampling results in higher spatial resolution and better image quality. Previous publications have described a more detailed technical background and evaluated the effect on image quality [8].

Iterative reconstruction is an image reconstruction algorithm that corrects for random fluctuations in photon measurements [9]. Formerly, iterative reconstruction was used in PET and single-photon CT [10, 11]. The most important role of iterative reconstruction is reducing image noise, which leads to better image quality. The effect of iterative reconstruction on the image noise and quality of CT images has been published previously [12–14]. For this study we used the adaptive statistical iterative reconstruction algorithm (ASiR; GE Healthcare, Waukesha, WI, USA) [9]. The purpose of this study was to clarify the effect of high-resolution mode and iterative reconstruction on computer-aided 3D volumetry.

Materials and methods

Phantom and nodules

The phantom used for this study was the anthropomorphic thoracic phantom Multipurpose Chest Phantom N1 "Lungman" (Kyoto Kagaku Inc., Japan). The phantom measures 43 × 40 × 48 cm in width, length and height. A picture of the phantom is shown in Fig. 1. A network of small structures attached to the heart/mediastinum is designed to mimic bronchial and vascular structures. The phantom does not contain a medium to mimic lung parenchyma and instead is filled with air. We used four spherical nodules with a density of +100 Hounsfield units and diameters of 5, 8, 10 and 12 mm.

The nodules were attached to the phantom using double-sided tape. Each nodule was scanned at 20 different locations, 10 times attached to the pleura and 10 times near vascular structures. The nodules with different sizes were placed at the same locations.

The diameter of each nodule was measured 100 times using a digital vernier calliper (0.01 mm). From the average diameter and the formula $V = (4/3)\pi r^3$, we calculated the assumed volume for each nodule.

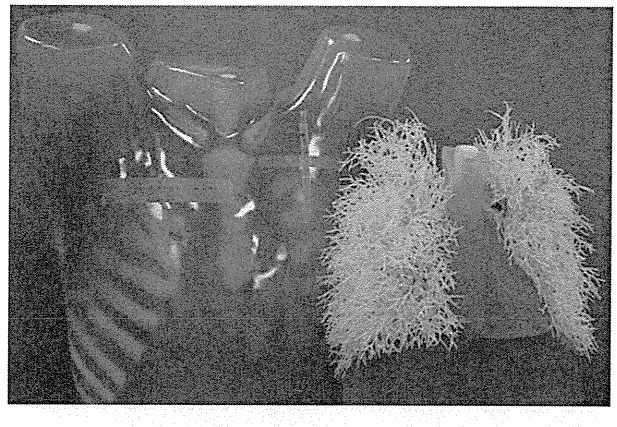

Fig. 1 A picture of the commercially available anthropomorphic thoracic phantom Multipurpose Chest Phantom N1 "Lungman" (Kyoto Kagaku Incorporated, Japan). The phantom is manufactured from urethane to mimics soft tissue and epoxy resins to mimic bone. On the *right side* we see the structure made to mimic the heart/mediastinum, which can be removed through the bottom of the phantom. Attached to the heart/mediastinum is a network of small structures designed to mimic the bronchus and vascular structures

Acquisition and analysis of CT images

For this study all scans were made using a multidetector CT capable of high-resolution mode (Discovery CT750HD, GE Healthcare, Milwaukee, WI, USA). CT scans were performed with either high-resolution or conventional scan mode. For the study we used the following scanning protocol: detector collimation, 64 × 0.625 mm; detector pitch, 0.984; gantry rotation, 0.5 s; matrix size, 512 × 512 pixels; field of view, 20 cm; tube voltage, 120 kVp; tube current for standard dose, 500 mA and for reduced radiation dose 120 mA.

We used the standard and reduced radiation dose to evaluate the effect of high-resolution mode and iterative reconstruction for different CT scanner settings. A field of view of 20 cm for each lung is the clinical standard at the institution where this study took place. Liu et al. [15] found that a minimum tube current necessary for characterisation of ground-glass opacity nodules was 120 mA. Following the ALARA principle we decided to use a tube current of 120 mA for the reduced radiation dose protocol. The CT scanner automatically selects a small or large focal spot size based on the tube voltage, tube current and conventional or high-resolution scan mode. For this study this resulted in a small focal spot size for the reduced radiation dose in both the conventional and high-resolution scan mode. For the normal radiation dose and conventional scan mode, the small focal spot was selected; the normal radiation dose and high-resolution mode resulted in a large

focal spot size. Axial thin-section CT images of 0.625 mm were created using a bone kernel. A high-spatial-frequency algorithm such as bone kernel is preferred as reconstruction kernel for pulmonary nodule volume reconstructions [7, 16]. The software allows blending of the iterative reconstruction with the FBP reconstruction. The amount of blending can be selected from 0 % (FBP image) in increasing steps of 10 % up to 100 % (pure iterative reconstruction image). For this study we used reconstructions of 0, 50 % and 100 % of iterative reconstruction blending.

Automatic 3D volumetry was performed with the software on the workstation (Lung VCAR; GE Healthcare Software). This software segments the pulmonary nodule by combining watershed segmentation and shape-analysis techniques [17]. The software automatically calculates the nodules volume after the centre of the nodule has been manually designated. In total, 960 patterns of the nodules [4 nodules (5, 8, 10 and 12 mm) × 4 scan protocols (high-resolution mode or conventional mode with 500 or 120 mA) × 3 iterative reconstruction techniques settings (0, 50 and 100 %) × 20 locations (10 locations attached to pleura and 10 locations attached to pulmonary vascular)] were analysed with 3D volumetry software.

Statistical analysis

We express our results in absolute percentage error (APE) and relative percentage error (RPE). We calculated the APE and RPE using the following formulas $APE = (|V_{ass.} - V_{cal.}|/V_{ass.}) \times 100$ and $RPE = (V_{cal.} - V_{ass.}/V_{ass.}) \times 100$. In these formulas $V_{ass.}$ is the assumed nodule volume and $V_{cal.}$ is the nodule volume calculated by the 3D volumetry software. The APE is calculated from the absolute difference between the assumed and calculated volume. Both over- and underestimation create a positive APE. In contrast, an underestimation creates a negative RPE. The APE indicates the error margin and the accuracy of the 3D volumetry. The RPE indicates the mean overestimation of the 3D volumetry. We used both the RPE and APE because an overestimation of 3D volumetry has been reported [7]. The use of APE and RPE allowed us to express our results with both accuracy and volume overestimation.

To compare the different scan modes, reconstruction algorithms, radiation doses and nodule sizes, a one-way ANOVA analysis with a post hoc Bonferroni test was used on APE and RPE. To compare pleural and vascular locations, we used an independent t test. A sub-analysis was made for high-resolution scan mode, ASiR blending and radiation dose using a paired t test. The database was created using the OpenOffice calculator (3.3). Statistical analysis was made with SPSS (17.0). A P value of <0.05 was considered significant.

Results

The assumed nodule volumes obtained from diameter measurements using vernier calliper are summarised in Table 1. An example series of 3D volumetry is shown in Fig. 2.

The results on APE from the 12 different scan and reconstruction patterns are summarised in Fig. 3. The smallest mean APE [5.8 % ± 13.1(SD)] was found in the normal radiation dose, high-resolution mode and 100 % iterative reconstruction blending pattern. The largest mean APE was seen in the normal radiation dose, conventional scan mode and 0 % iterative reconstruction blending (11.5 % ± 39.8). Statistical analysis between the individual patterns showed no significant difference for mean APE or RPE. The mean APE for all 3D volumetry from all patterns was 7.5 % ± 21.3. The mean RPE for all 3D volumetry was 5.6 % ± 21.9.

The effect of nodule size and location

The effects of nodule size on mean APE are summarised in Table 2. APE of the nodule with the 5 mm diameter was 19.1 %, which was significantly higher compared to the nodules with 8, 10 and 12 mm diameters ($P < 0.001$). The difference between the other nodules sizes was not significant. Statistical analysis of RPE showed a similar result.

Table 1 Assumed volume for nodule calculated from 100 diameter measurements

	Assumed nodule volume			
	Mean diameter (mm)	Mean volume (mm^3)	SD from nodule volume	N
Nodule 5 mm	5.0	65	1.7	100
Nodule 8 mm	7.9	262	2.4	100
Nodule 10 mm	10.0	516	3.1	100
Nodule 12 mm	12.0	895	7.1	100

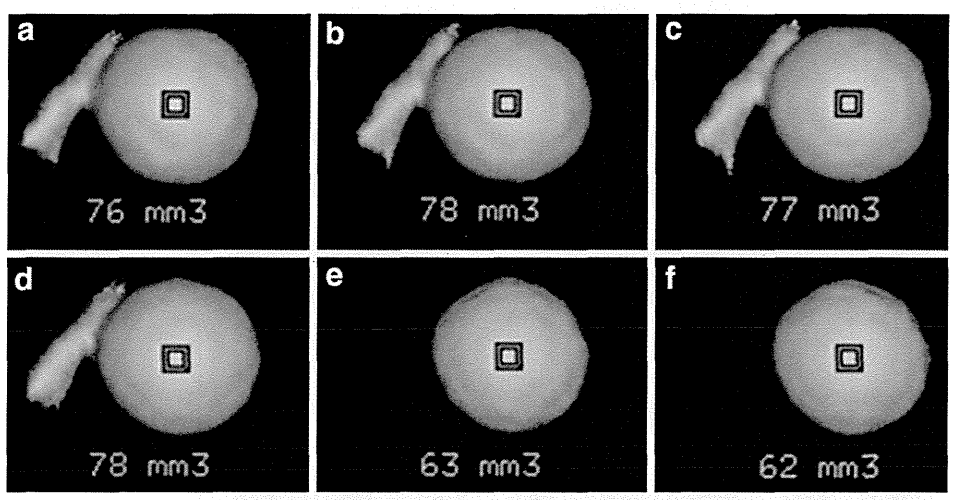

Fig. 2 An example of 3D volumetry from a pulmonary nodule with 5 mm diameter (assumed volume 65 mm^3). The *number* underneath the nodule represents the calculated volume. All reconstructions are made using a tube current of 500 mA. **a** Conventional scan mode 0 % iterative reconstruction; **b** conventional scan mode 50 % iterative reconstruction; **c** conventional scan mode 100 % iterative reconstruction; **d** high-resolution mode 0 % iterative reconstruction; **e** high-resolution mode 50 % iterative reconstruction; **f** high-resolution mode 100 % iterative reconstruction. In this example there is a clear improvement of the 3D volumetry for the high-resolution 50 and 100 % iterative reconstruction. Please note that this figure is added as an illustration of an individual 3D volumetry and does not represent the complete outcome of this study

The APE from nodules attached to the pleura (6.1 % ± 6.9) was significantly lower compared to nodules attached to vascular structures (8.9 % ± 29.3) ($P = 0.044$).

The effect of radiation dose

The effect of reduced radiation dose on the mean APE and RPE is summarised in Fig. 4.

The reduced radiation dose had a lower APE (7.4 % ± 21.5) compared to the normal radiation dose (7.6 % ± 21.2), but this difference was not significant ($P = 0.559$). However, the RPE showed a significant difference between reduced (4.8 % ± 22.2) and normal (6.4 % ± 21.6) radiation dose ($P < 0.001$).

The effect of iterative reconstruction

Analysis of iterative reconstruction blending resulted in a mean APE of 8.8 % ± 27.9, 7.1 % ± 16.4 and 6.6 % ± 17.8 for 0, 50 and 100 % iterative reconstruction, respectively, and statistical analysis showed no significant difference. The results for RPE were similar to those from the APE, with a mean RPE of 7.0 % ± 28.4, 5.2 % ± 17.1 and 4.7 % ± 18.4 for 0, 50 and 100 % iterative reconstruction blending, respectively, and statistical analysis of the RPE also showed no significant difference.

When looking at Fig. 3, we suspect the effect of iterative reconstruction is larger in the reconstructions made with the conventional scan mode. We made a separate paired *t* test to compare the effect of iterative reconstruction within the conventional scan mode for both the normal and reduced radiation setting. This sub-analysis also resulted in a non-significant reduction in APE and RPE.

The effect of high-resolution mode

The effect of high-resolution mode on the mean APE and RPE is shown in Fig. 5. APE of the high-resolution mode (6.6 % ± 17.1) was lower compared to that of the conventional scan mode (8.3 % ± 24.9), but this difference was not significant ($P = 0.066$). However, the mean RPE of high-resolution mode (4.4 % ± 17.8) was significantly ($P < 0.05$) lower than that of the conventional scan mode (6.9 % ± 25.3).

Discussion

Previous studies showed that tube current, reconstruction kernel, slice thickness and nodule size influenced the result on 3D volumetry [6, 7, 15–17]. In this study, the 3D volumetry from all scan and reconstruction patterns resulted in overestimation of the mean calculated volume, especially in small nodules. The 3D volumetry from the 5-mm-diameter nodule was less accurate than those of larger nodules; the effect of increasing inaccuracy with declining nodule size has previously been published [6, 7]. There are two assumptions for this effect. First, the volume error may result from the inaccurate volume measurement of the peripheral part of the nodule by nodule segmentation. If the

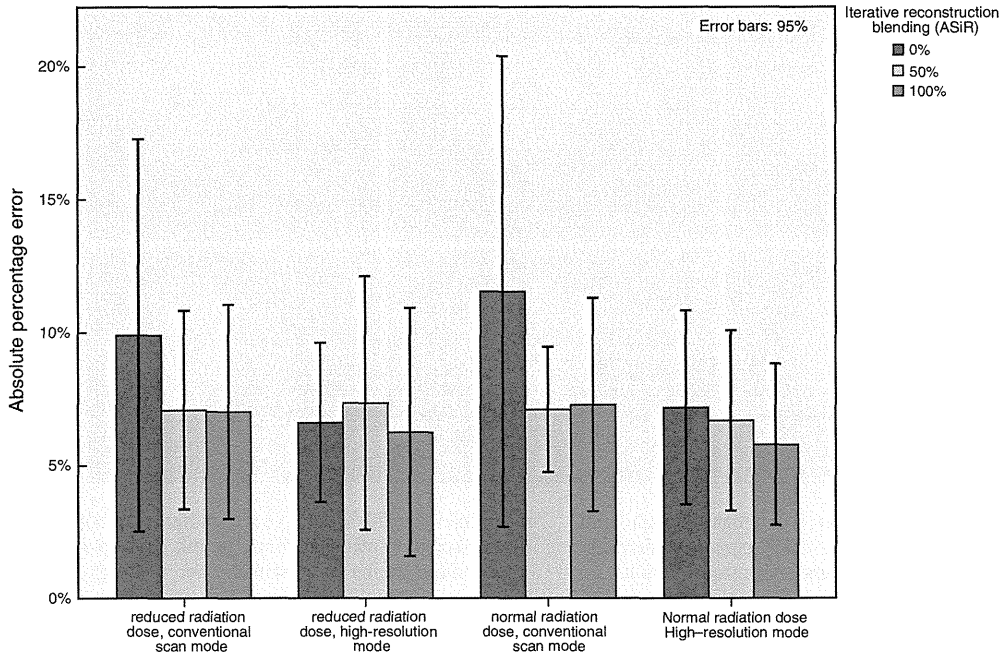

Fig. 3 Absolute percentage error (APE) for the 12 different 3D volumetry patterns. *Each bar* represents the mean APE and is made from 80 3D volumetry reconstructions, resulting in a total of 960 3D volumetry reconstructions. The 95 % error margin is indicated by the *line* on *top* of *each bar*. The difference between these individual patterns is not significant

Table 2 The absolute percentage error for different nodule sizes

Diameter	Mean APE	SD	*N*
Absolute percentage error			
5 mm	19.1	39.7	240
8 mm	4.6	6.6	240
10 mm	3.8	4.3	240
12 mm	2.4	2.4	240
Total	7.5	21.3	960

size of the pulmonary nodule is small, a large part of the nodule will be influenced by the inaccurate segmentation. Therefore, the ratio of the volume error becomes larger in small pulmonary nodules even if the volume error of the small nodule is tiny compared to that of the large nodule. The second assumption was the segmentation error of the nodule from surrounding structures. If the size of the nodule is small, the segmentation of the nodule becomes difficult on 3D volumetry software. In that case, the normal structures such as pulmonary vessels or pleura cannot be removed from the true pulmonary nodule, and the calculated nodule volume contains pulmonary vessels of pleura, which leads to overestimation. In conclusion, we must take care in evaluating small pulmonary nodules by 3D volumetry software.

In our study, there was no significant difference between reduced radiation doses and normal radiation doses in APE, but the RPE in reduced radiation doses was significantly lower than in normal radiation doses. Linning et al. [18] documented that there was no significant difference in APE while there was a significant difference in RPE, and there was substantial underestimation at 30, 60 and 90 mA and substantial overestimation at 120, 150, 180 and 210 mA of tube current on volumetric measurement of ground-glass opacity nodules using a chest phantom. When observing the 3D volumetry from the reduced radiation dose patterns, we saw that the surface was irregular and had numerous small holes in it, giving it a "golf ball"-like appearance. Possibly these surface irregularities occur because of increased noise and decreased spatial resolution, making segmentation of the surface more difficult. A reduced radiation dose may have the effect of making the calculated nodule volume smaller compared to a normal radiation dose.

Surprisingly, a non-significant reduction in error margin and volume overestimation in the 3D volumetry was obtained with iterative reconstruction. We hypothesised that the noise reduction effect of iterative reconstruction contributed to the improvement of accurate volume measurement. Though there was no statistical difference in this study, the mean APE and mean RPE were reduced when using iterative reconstruction. When looking at our data we found the effect of iterative reconstruction to be most prominent in the conventional scan mode. Possibly the increased spatial resolution from the high-resolution mode

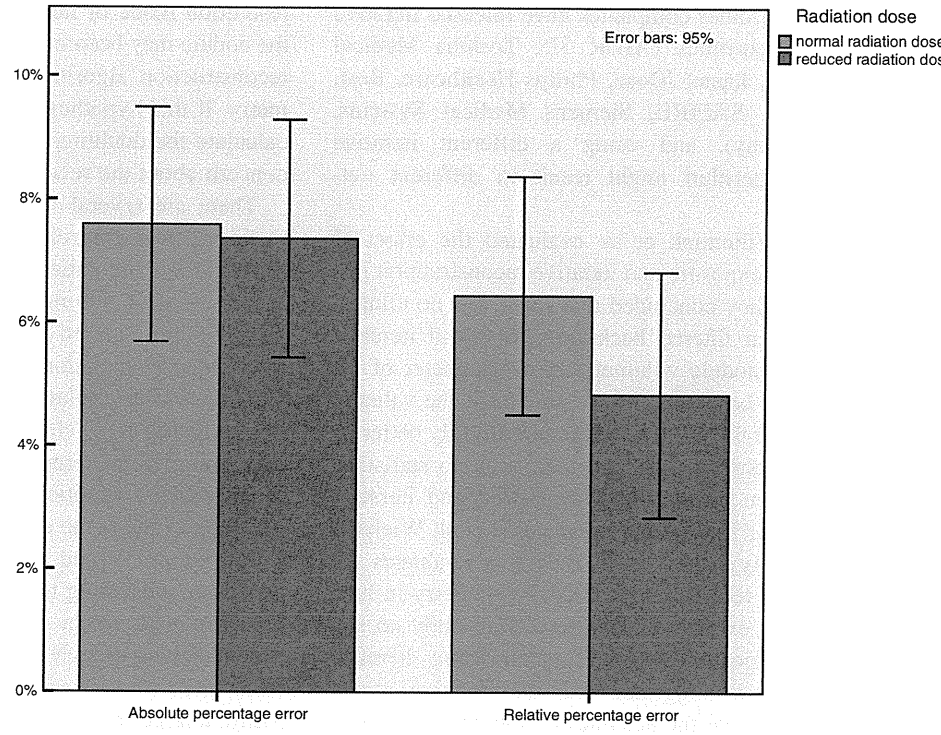

Fig. 4 Absolute and relative percentage error for normal and reduced radiation dose. *Each bar* is made from 480 3D volumetry reconstructions. The 95 % error margin is indicated by the *line* on *top* of *each bar*. The difference in APE is not significant. The RPE of the reduced radiation dose is significantly lower than the RPE from the normal radiation dose

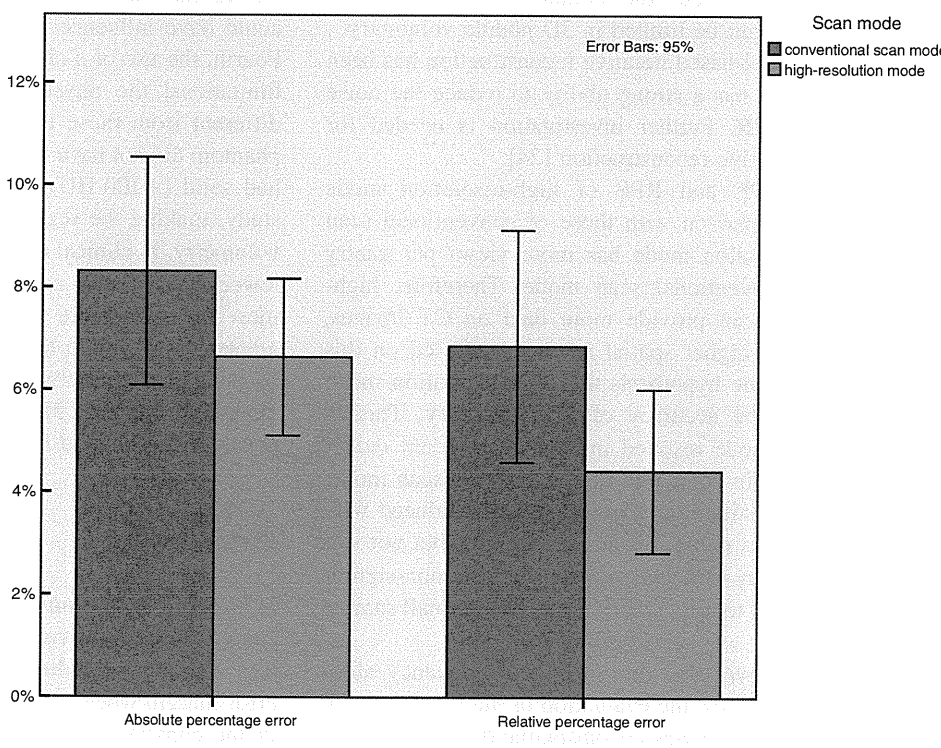

Fig. 5 Absolute and relative percentage error for conventional scan mode and high-resolution scan mode. *Each bar* is made from 480 3D volumetry reconstructions. The difference in APE is not significant ($P = 0.066$); the difference in RPE is significant ($P = 0.011$)

reduces the effect of iterative reconstruction on 3D volumetry. Therefore, we also evaluated the effect of iterative reconstruction in the conventional scan mode; however, this effect was also non-significant. This result may be due to the small sample size, and possibly a larger sample size will result in a significant reduction. When we saw some individual cases, iterative reconstruction resulted in important improvements.

It is important to note that ASiR was used to evaluate the effect of iterative reconstruction on 3D volumetry in

our study. Several other companies have released iterative reconstruction algorithms (AIDR 3D, Toshiba Medical Systems Otawara, Japan; iDose, Philips Healthcare, Best, The Netherlands; SAFIRE, Siemens Medical Systems, Erlangen, Germany), and using a different iterative reconstruction algorithm might result in different outcomes. [19–21].

A study by Willemink et al. evaluated the effect of reduced radiation exposure and iterative reconstruction in a phantom study. They concluded that there was no clinical difference between filtered back projection and iterative reconstruction in nodule volumetry if the diameter of the nodule was 5 mm or larger [22]. In our study, the value of the mean APE and the mean RPE became slightly better by using iterative reconstruction, but there was no statistical difference between filtered back projection and iterative reconstruction as in the study by Willemink et al. Wielpütz et al. [23] recently published a study that evaluates the effect of iterative reconstruction on 3D volumetry in lung nodules placed in ex vivo pig lungs. In this study no significant improvement was found when using iterative reconstruction. It is suggested that the iterative reconstruction may improve the accuracy of the calculated volume in some cases, but the influence of the iterative reconstruction might be limited in 3D nodule volumetry.

Recently, model-based iterative reconstruction has been developed, which has a strong ability to reduce the noise compared to ASiR. Further investigation is needed for model-based iterative reconstruction [24].

The mean APE and RPE of high-resolution mode improved in comparison with those of conventional scan mode. High-resolution mode has more views per gantry rotation than conventional scan mode. Therefore, high-resolution mode can provide more data on CT images, which leads to a higher spatial resolution. Based on this idea we formed the hypothesis that high-resolution mode would increase the accuracy of 3D volumetry. Though high-resolution mode resulted in a non-significant reduction in error margin compared to conventional scan mode, the volume overestimation was significantly reduced with the high-resolution mode. Because of the low but not significant P value in APE, we suspect that this non-significant result in error margin could be due to the small sample size.

In this study, we used only one high-frequency algorithm (bone kernel) for the evaluation of 3D volumetry. In a phantom study, there was no substantial difference in the accuracy of volume estimations across the seven reconstruction kernels including bone and standard algorithm [7]. However, the measured volume with a low-frequency algorithm (standard algorithm) being smaller than that with a high-frequency algorithm (bone algorithm) has been reported in a clinical study [16]. When using high-resolution mode or iterative reconstruction, the margin of the nodule may become more clear, and the influence of the reconstruction algorithm might be reduced on 3D volumetry. If this hypothesis is proven, it would be possible to calculate the doubling time of pulmonary nodules without concern about the reconstruction algorithm.

There are several limitations in our study. First, automatic exposure control (AEC) is used to lower the radiation exposure for the patient in the clinical setting. Our fixed tube current of 500 mA was relatively high compared to the tube current used in clinical settings using AEC [25]. The reduced radiation protocol with a tube current of 120 mA was also relatively high compared to low or ultra-low radiation AEC chest CT scans [26]. In this study, we used these two patterns of tube currency to try to eliminate the effect of a variation in radiation dose. Further investigation to evaluate the effect in ultra-low dose CT is needed in the future. Second, we found small variations in diameter when measuring the nodule diameter using the vernier calliper, resulting in a variation in the assumed nodule volume. Even though this difference was small, it is possible there was an error in the assumed nodule volume. Third, a large focal spot size was automatically selected in the normal radiation dose and high-resolution mode; this could have influenced the outcome of the 3D volumetry. Fourth, the use of a chest phantom results in several study limitations; the physical properties of the phantom are different from those in actual patients; among others, the phantom did not have breathing artefacts. Fifth, the nodules had solid (+100 HU) density and spherical shape in this study, making the segmentation of the nodule easy in 3D volumetry. In clinical practice non-spherical nodules with a lower density (for example, ground-glass nodules) will most likely be more difficult to segment and result in a greater error margin than observed in this phantom study. Sixth, only one software was used in this study for 3D volumetry. Another 3D volumetry software might produce different results, and further investigation is needed.

Conclusion

In this phantom study, the high-resolution mode significantly reduced the volume overestimation of 3D volumetry. We found a reduction in volume overestimation and error margin when using iterative reconstruction especially in the conventional scan mode; however, this effect was not significant.

Acknowledgments We thank the CT technicians of the Osaka University Radiology Department for support with the CT scanner. We thank Dr. J.R. Huizenga and S. Babab MD PhD for their support and work in the International Department for Medical students of the University of Groningen and Osaka University respectively.

Conflict of interest The authors declare that they have no conflict of interest.

References

1. Parkin DM. Global cancer statistics in the year 2000. Lancet Oncol. 2001;2:533–43.
2. Yankelevitz DF, Henschke CI. Does 2-year stability imply that pulmonary nodules are benign? AJR Am J Roentgenol. 1997;168:325–8.
3. Ashraf H, Dirksen A, Loft A, Bertelsen AK, Bach KS, Hansen H, et al. Combined use of positron emission tomography and volume doubling time in lung cancer screening with low-dose CT scanning. Thorax. 2011;66:315–9.
4. Eisenhauer EA, Therasse P, Bogaerts J, Schwartz LH, Sargent D, Ford R, et al. New response evaluation criteria in solid tumours: revised RECIST guideline (version 1.1). Eur J Cancer. 2009;45:228–47.
5. Jennings SG, Winer-Muram HT, Tarver RD, Farber MO, et al. Lung tumor growth: assessment with CT—comparison of diameter and cross-sectional area with volume measurements. Radiology. 2004;231:866–71.
6. Ko JP, Rusinek H, Jacobs EL, Babb JS, Betke M, McGuinness G, et al. Small pulmonary nodules: volume measurement at chest CT—phantom study. Radiology. 2003;228:864–70.
7. Ravenel JG, Leue WM, Nietert PJ, Miller JV, Taylor KK, Silvestri GA, et al. Pulmonary nodule volume: effects of reconstruction parameters on automated measurements—a phantom study. Radiology. 2008;247:400–8.
8. Yanagawa M, Tomiyama N, Honda O, Kikuyama A, Sumikawa H, Inoue A, et al. Multidetector CT of the lung: image quality with garnet-based detectors. Radiology. 2010;255:944–54.
9. Silva AC, Lawder HJ, Hara A, Kujak J, Pavlicek W, et al. Innovations in CT dose reduction strategy: application of the adaptive statistical iterative reconstruction algorithm. AJR Am J Roentgenol. 2010;194:191–9.
10. Knesaurek K, Machac J, Vallabhajosula S, Buchsbaum MS. A new iterative reconstruction technique for attenuation correction in high-resolution positron emission tomography. Eur J Nucl Med. 1996;23:656–61.
11. Wells RG, King MA, Simkin PH, Judy PF, Brill AB, Gifford HC, et al. Comparing filtered backprojection and ordered-subsets expectation maximization for small-lesion detection and localization in 67 Ga SPECT. J Nucl Med. 2000;41:1391–9.
12. Leipsic J, Nguyen G, Brown J, Sin D, Mayo JR. A prospective evaluation of dose reduction and image quality in chest CT using adaptive statistical iterative reconstruction. AJR Am J Roentgenol. 2010;195:1095–9.
13. Yanagawa M, Honda O, Yoshida S, Kikuyama A, Inoue A, Sumikawa H, et al. Adaptive statistical iterative reconstruction technique for pulmonary CT: image quality of the cadaveric lung on standard- and reduced-dose CT. Acad Radiol. 2010;17:1259–66.
14. Prakash P, Kalra MK, Ackman JB, Digumarthy SR, Hsieh J, Do S, et al. Diffuse lung disease: CT of the chest with adaptive statistical iterative reconstruction technique. Radiology. 2010;256:261–9.
15. Liu D, Awai K, Funama Y, Oda S, Nakaura T, Yanaga Y, et al. Identification and characterization of focal ground-glass opacity in the lungs by high-resolution CT using thin-section multidetector helical CT: experimental study using a chest CT phantom. Radiat Med. 2008;26:21–7.
16. Honda O, Johkoh T, Sumikawa H, Inoue A, Tomiyama N, Mihara N, et al. Pulmonary nodules: 3D volumetric measurement with multidetector CT—effect of intravenous contrast medium. Radiology. 2007;245:881–7.
17. Revel MP, Lefort C, Bissery A, Bienvenu M, Aycard L, Chatellier G, et al. Pulmonary nodules: preliminary experience with three-dimensional evaluation. Radiology. 2004;231:459–66.
18. Linning E, Daqing M. Volumetric measurement pulmonary ground-glass opacity nodules with multi-detector CT: effect of various tube current on measurement accuracy—a chest CT phantom study. Acad Radiol. 2009;16:934–9.
19. Yamada Y, Jinzaki M, Hosokawa T, Tanami Y, Sugiura H, Abe T, et al. Dose reduction in chest CT: comparison of the adaptive iterative dose reduction 3D, adaptive iterative dose reduction, and filtered back projection reconstruction techniques. Eur J Radiol. 2012;81(12):4185–95.
20. Noël PB, Fingerle AA, Renger B, Münzel D, Rummeny EJ, Dobritz M. Initial performance characterization of a clinical noise-suppressing reconstruction algorithm for MDCT. AJR Am J Roentgenol. 2011;197:1404–9.
21. Yang WJ, Yan FH, Liu B, Pang LF, Hou L, Zhang H, et al. Can sinogram-affirmed iterative (SAFIRE) reconstruction improve imaging quality on low-dose lung ct screening compared with traditional filtered back projection (FBP) reconstruction? J Comput Assist Tomogr. 2013;37:301–5.
22. Willemink MJ, Leiner T, Budde RP, de Kort FP, Vliegenthart R, van Ooijen PM, et al. Systematic error in lung nodule volumetry: effect of iterative reconstruction versus filtered back projection at different CT parameters. AJR Am J Roentgenol. 2012;199:1241–6.
23. Wielpütz MO, Lederlin M, Wroblewski J, Dinkel J, Eichinger M, Biederer J, et al. CT volumetry of artificial pulmonary nodules using an ex vivo lung phantom: influence of exposure parameters and iterative reconstruction on reproducibility. Eur J Radiol. 2013;. doi:10.1016/j.ejrad.035.
24. Katsura M, Matsuda I, Akahane M, Yasaka K, Hanaoka S, Akai H, et al. Model-based iterative reconstruction technique for ultralow-dose chest CT: comparison of pulmonary nodule detectability with the adaptive statistical iterative reconstruction technique. Invest Radiol. 2013;48:206–12.
25. Mulkens TH, Bellinck P, Baeyaert M, Ghysen D, Van Dijck X, Mussen E, et al. Use of an automatic exposure control mechanism for dose optimization in multi-detector row CT examinations: clinical evaluation. Radiology. 2005;237:213–23.
26. Aberle DR, Berg CD, Black WC, Church TR, Fagerstrom RM, Galen B, et al. The National Lung Screening Trial: overview and study design. Radiology. 2011;258:243–53.

Cancer Chemother Pharmacol (2013) 72:1283–1290
DOI 10.1007/s00280-013-2306-7

ORIGINAL ARTICLE

Goshajinkigan oxaliplatin neurotoxicity evaluation (GONE): a phase 2, multicenter, randomized, double-blind, placebo-controlled trial of goshajinkigan to prevent oxaliplatin-induced neuropathy

Toru Kono · Taishi Hata · Satoshi Morita · Yoshinori Munemoto · Takanori Matsui · Hiroshi Kojima · Hiroyoshi Takemoto · Mutsumi Fukunaga · Naoki Nagata · Mitsuo Shimada · Junichi Sakamoto · Hideyuki Mishima

Received: 31 March 2013 / Accepted: 25 September 2013 / Published online: 12 October 2013

Abstract
Purpose Oxaliplatin-induced peripheral neurotoxicity (OPN) is frequent and potentially severe, but successful treatment of this condition is still an unmet clinical need. We aimed to determine whether treatment with goshajinkigan (TJ-107), a traditional Japanese medicine, is better than placebo in preventing OPN in patients with advanced or recurrent colorectal cancer patients treated with standard FOLFOX regimens.
Methods In this phase 2, randomized, double-blind, placebo-controlled study, patients undergoing oxaliplatin-based chemotherapy were randomized to receive either oral TJ-107 (7.5 g) or matching placebo daily. The severity of OPN was assessed according to the Common Toxicity Criteria for Adverse Events at baseline, every 2 weeks until the 8th cycle, and every 4 weeks thereafter until the 26th week. The primary endpoint was the incidence of grade 2 or greater OPN until the 8th cycle of chemotherapy.
Results Analyses were done by intention to treat. Eighty-nine patients were randomly assigned to receive either TJ-107 ($n = 44$) or placebo ($n = 45$) between May 2009 and March 2010. The incidence of grade 2 or greater OPN until the 8th cycle was 39 and 51 % in the TJ-107 and placebo groups, respectively (relative risk (RR), 0.76; 95 % CI, 0.47–1.21). The incidence of grade 3 OPN was 7 % (TJ-107) vs. 13 % (placebo) (0.51, 0.14–1.92). No concerns regarding toxicity emerged with TJ-107 treatment.
Conclusions TJ-107 appears to have an acceptable safety margin and a promising effect in delaying the onset of grade 2 or greater OPN without impairing FOLFOX efficacy.

Keywords Goshajinkigan · Peripheral neuropathy · Double-blind randomized trial · Oxaliplatin · Colorectal cancer

Findings from this study have been partially presented at the 36th European Multidisciplinary Cancer Congress (EMCC), September 23–27, 2011, Stockholm, Sweden; Multinational Association of Supportive Care in Cancer/International Symposium on Supportive Care in Cancer 2011 (MASCC/ISOO 2011), June 23–25, 2011, Athens, Greek; 13th World Congress on Gastrointestinal Cancer, June 22–25, 2011, Barcelona, Spain; and American Society of Clinical Oncology (ASCO) 47th Annual Meeting 2011, June 1–15, 2011, Chicago, USA.

Taishi Hata contributed equally as co-first author of this manuscript

T. Kono (✉)
Advanced Surgery Center, Sapporo Higashi Tokushukai Hospital, Sapporo, 3-1, N33, E 14, Higashi-ku, Hokkaido 065-0033, Japan
e-mail: kono@toru-kono.com

T. Hata
Department of Gastroenterological Surgery, Osaka University, Graduate School of Medicine, Suita, Osaka 565-0871, Japan

S. Morita
Department of Biostatistics and Epidemiology, Yokohama City University Medical Center, Yokohama, Kanagawa 232-0024, Japan

Y. Munemoto
Department of Surgery, Fukuiken Saiseikai Hospital, Wadanaka-cho, Fukui 918-8503, Japan

T. Matsui · H. Kojima
Department of Surgery, Aichi Cancer Center, Aichi Hospital, Okazaki, Aichi 444-0011, Japan

H. Takemoto · M. Fukunaga
Department of Surgery, Sakai Municipal Hospital, Sakai, Osaka 590-0064, Japan

Introduction

Oxaliplatin is considered one of the gold standard chemotherapeutic agents for advanced colorectal cancers and for adjuvant chemotherapy. However, oxaliplatin-induced peripheral neurotoxicity (OPN) is extremely common with the incidence varying from 82 to 98 % [1–3]. Severe OPN occurs in 10 to 20 % of patients [1, 4], and some may require dose reductions and discontinuation of treatment, potentially reducing the efficacy of chemotherapy and survival [5–7]. Despite considerable efforts to discover neuroprotective agents to prevent OPN [8], the best pharmacologic strategy for the management of OPN remains controversial [9–11].

In Japan, TJ-107 (goshajinkigan), a traditional Japanese medicine (Kampo) [12], has been frequently prescribed to alleviate symptoms of diabetic peripheral neuropathy such as numbness, cold sensation, and paresthesias/dysesthesias [13–15]. We hypothesized that TJ-107 might be effective against OPN and retrospectively investigated its use in a pilot study of 90 patients with advanced colorectal cancer undergoing FOLFOX therapy [16]. Patients were treated with TJ-107, calcium (Ca) gluconate and magnesium (Mg) sulfate infusion, combination of TJ-107 and Ca/Mg infusion, or chemotherapy alone. Our results showed that the group receiving TJ-107 with FOLFOX regimen experienced significant improvement in OPN and showed a favorable safety profile. We subsequently conducted a small, single-arm prospective study in 45 patients who were treated with modified FOLFOX6 for advanced colorectal cancer, in which 22 patients receiving oral TJ-107 reported lower incidence of grades 2 and 3 OPN than that in the control group [17]. Hence, this phase 2, randomized, double-blind, placebo-controlled, exploratory trial was initiated to investigate the neuroprotective effect of TJ-107 for OPN.

N. Nagata
Department of Surgery, Kitakyushu General Hospital, Kitakyushu, Fukuoka 800-0295, Japan

M. Shimada
Department of Surgery, Institute of Health Biosciences, The University of Tokushima Graduate School of Medicine, Tokushima, Tokushima 770-8503, Japan

J. Sakamoto
Tokai Central Hospital, Kagamihara, Gifu 504-8601, Japan

H. Mishima
Unit of Cancer Center, Aichi Medical University, Nagakute, Aichi 480-1195, Japan

Methods

Study design

This was an exploratory, randomized, phase 2 trial to evaluate the efficacy of TJ-107 for preventing OPN in the Goshajinkigan Oxaliplatin Neurotoxicity Evaluation (GONE) study group conducted at 20 institutions in Japan [18].

Eligibility criteria

Patients were eligible if they had histologically confirmed colorectal cancer and were scheduled to undergo chemotherapy with infusional 5-fluorouracil (5-FU), leucovorin (*l*-LV), and oxaliplatin (either FOLFOX4 or modified FOLFOX6 regimen). Patients had to have a good performance status (ECOG 0–1), adequate bone marrow function (WBC $\geq$ 3,000 and $\leq$12,000/mm^3, neutrophil count $\geq$ 1,500/mm^3, platelet count $\geq$100,000/mm^3), renal function (serum creatinine level less than the institutional upper limit of normal), and hepatic function (bilirubin $\leq$ 1.5 times institutional normal, aspartate aminotransferase, and alanine aminotransferase levels less than 2.5 times the institutional upper limit of normal), life expectancy $\geq$12 weeks, without evidence of clinical infection, and without preexisting peripheral neuropathy from any cause. Exclusion criteria included prior exposure to chemotherapy, except for oral fluorinated pyrimidine derivatives or 5-FU/*l*-LV in an adjuvant setting, use of other Kampo medicines, history of severe hypersensitivity (allergy) to any medications, other active malignancies or a history of other malignancies within the past 5 years, congestive heart failure, diabetes, or a history of a hemorrhagic stroke. Patients who were pregnant or nursing, taking a neuropathic pain medication, or receiving radiation were deemed ineligible.

This study was conducted in accordance with the Declaration of Helsinki and the Japanese Ministry of Health, Labour and Welfare guidelines, and informed consent was obtained from all participants. The study protocol was approved by the local Institutional Review Board at each participating institution.

Randomization and masking

Eligible patients were centrally randomized by a computer-generated allocation sequence in a 1:1 ratio to either TJ-107 group or placebo group. Information regarding the necessary follow-up tests was then sent to the registration center at the non-profit organization Epidemiological and Clinical Research Information Network (ECRIN). Patients, investigators, and data collectors were all blinded to treatment allocation.

Study medications

TJ-107 is a mixture of aqueous extracts from 10 crude herbs in fixed proportions (Rehmanniae Radix, 10.7 %; Achyranthis Radix, 6.4 %; Corni Fructus, 6.4 %; Moutan Cortex, 6.4 %; Alismatis Rhizome, 6.4 %; Dioscoreae Rhizome, 6.4 %; Plantaginis Semen, 6.4 %; Poria (*Poria cocos* Wolf), 6.4 %; processed Aconiti Tuber, 2.1 %; and Cinnamomi Cortex, 2.1 %). The extract powder of TJ-107 is commercially available in Japan and was obtained from Tsumura & Co. (Tokyo, Japan). Matching placebo (Tsumura & Co.) was specifically manufactured for this clinical trial. The appearance, color, and odor of the placebo were well controlled that both patients and clinicians were unable to distinguish this placebo from the original TJ-107. Dried powder (2.5 g) of TJ-107 or placebo was administered orally three times a day before each meal (7.5 g/day).

Treatment

Patients were randomly assigned to receive TJ-107 or placebo with either FOLFOX4 or mFOLFOX6 therapy. This treatment was initiated at the first delivery of FOLFOX and continued throughout the administration of chemotherapy and for 26 weeks beyond the completion of chemotherapy. Cycles of chemotherapy were given every 2 weeks until progressive disease or unacceptable toxicity occurred.

TJ-107 was given orally for 26 weeks starting on the day of oxaliplatin infusion. To avoid any possible influence on the assessment of neurotoxicity, Ca/Mg infusion was prohibited only during the 26-week administration of TJ-107 and not throughout the chemotherapy regimen. FOLFOX4 therapy consisted of infusion of *l*-LV at 100 mg/m^2 over 2 h followed by 5-FU as a bolus (400 mg/m^2) and a 22-h infusion of 5-FU (600 mg/m^2) on day 1 and day 2, with infusion of oxaliplatin at 85 mg/m^2 over 2 h on day 1. This regimen was repeated every 2 weeks. mFOLFOX6 therapy consisted of infusion of *l*-LV at 200 mg/m^2 over 2 h followed by 5-FU as a bolus (400 mg/m^2) and a 46-h infusion of 5-FU (2,400 mg/m^2) with an infusion of oxaliplatin at 85 mg/m^2 over 2 h on day 1. This regimen was repeated every 2 weeks.

Adverse reactions including OPN were assessed at baseline (prior to starting FOLFOX + TJ-107 or FOLFOX + placebo), every 2 weeks until the 8th cycle and every 4 weeks thereafter until the 26th week according to the National Cancer Institute Common Terminology Criteria for Adverse Events (NCI-CTCAE v3.0). The severity of neurotoxicity was assessed by the study clinicians who were blinded to treatment allocation and used the sensory neuropathy items in NCI-CTCAE v3.0, which describe the four grades as follows: grade 1, loss of deep tendon reflexes or paresthesia, including tingling, but not interfering with function; grade 2, objective sensory alteration or paresthesia, including tingling, interfering with function, but not interfering with activities of daily living (ADL); grade 3, sensory alteration or paresthesia interfering with ADL; and grade 4, permanent sensory losses that are disabling. In addition, patients rated their symptoms on a 0–4 scale using the Functional Assessment of Cancer Therapy/Gynecological Oncology Group-Neurotoxicity (FACT/GOG-Ntx-12) score at screening, at baseline, and before each chemotherapy treatment. These subjective ratings were independently evaluated from the clinician-rated CTCAE grading. The follow-up period was 1 year after registration of the last patient.

Statistical analysis

The primary endpoint of this study was the incidence of grade 2 or greater OPN after 8 cycles of chemotherapy as assessed by the clinical investigators. The rate of incidence was compared between evaluable patients randomized to either the TJ-107 or the placebo group. The rate of occurrence of grade 2 or greater OPN was calculated for each group and compared using the chi-square test.

Secondary endpoints included the incidence and grading of OPN after each cycle, FACT/GOG-Ntx-12 score, time to occurrence of OPN, response rate to chemotherapy, and toxicity.

Previously, we found that the incidence of grade 2 or greater OPN was 15 and 45 % (TJ-107 vs placebo) from the start of oxaliplatin treatment until the completion of cycle 8 [16]. On the basis of this data, we determined that in order to detect with 80 % power while maintaining a significance level of 10 % in a two-sided test, 35 patients per group would be required to compare the two treatment groups with a chi-square test. To account for possible dropouts, a minimum of 40 patients were enrolled in each group (80 in total). Randomization was achieved by using three strata: use of bevacizumab, the institution, and the presence of target lesions evaluated by Response Evaluation Criteria in Solid Tumors (RECIST) version 1.1. This trial is registered with the UMIN Clinical Trials Registry in Japan (UMIN000002211).

Results

A total of 93 patients were enrolled from May 1, 2009, to March 31, 2010. Of the 93 patients, 47 were assigned to the TJ-107 group and 46 to the placebo group. Four patients (3 receiving TJ-107 and 1 control) were withdrawn before initiation of treatment and included in the intention-to-treat set analysis (Fig. 1). The remaining 89 (96 %) patients were consequently assessable for efficacy

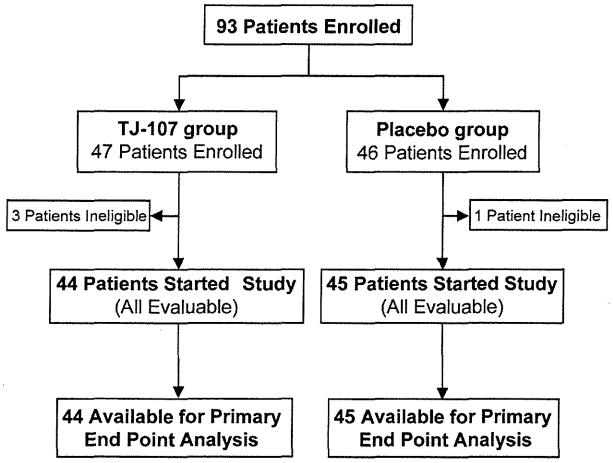

Fig. 1 CONSORT diagram

Table 1 Patient characteristics

	TJ-107 ($N = 44$)	Placebo ($N = 45$)	P value
Sex			
Male	23	25	0.833
Female	21	20	
Age			
Median	67	61	0.215
Range	40–88	36–82	
Performance status			
0	40	44	0.203
1	4	1	
Primary tumor			
Colon	28	30	0.826
Rectum	16	15	
Chemotherapy			
First-line	36	35	0.793
Adjuvant	8	10	

and toxicity. Reasons for premature withdrawal were disease progression (6 patients), adverse events (4), medical reasons (4), patient request (2), and complete response, operation, or death (1 each). Generally, demographic and background characteristics of the patients were well balanced between the TJ-107 group ($n = 44$) and placebo group ($n = 45$) (P values ranging from 0.203–0.833) (Table 1).

Incidence of OPN

Data on the incidence of grade 2 or greater OPN and grade 3 OPN until the 8th cycle are summarized (Table 2). The incidence of grade 2 or greater OPN until the 8th cycle was 39 % in the TJ-107 group and 51 % in the placebo group (relative risk (RR) 0.76; 95 % confidence interval (CI) 0.47–1.21). Similarly, the incidence of grade 3 OPN until the 8th cycle was 7 % in the TJ-107 group and 13 % in the placebo group (RR 0.51; 95 %CI 0.14–1.92).

Table 2 Oxaliplatin-induced peripheral neurotoxicity until the 8th cycle

Oxaliplatin-induced peripheral neurotoxicity until the 8th cycle			
	TJ-107 ($N = 44$) (%)	Placebo ($N = 45$) (%)	Relative risk [95 %CI]
Grade ≥2	39	51	0.76 [0.47–1.21]
Grade 3	7	13	0.51 [0.14–1.92]

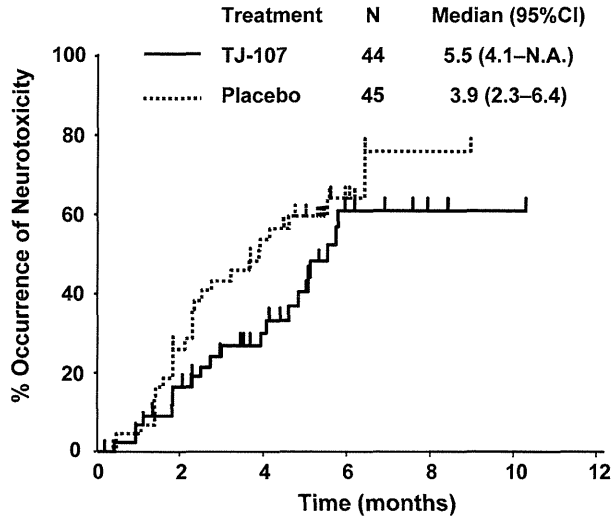

Fig. 2 Time to occurrence of grade 2 or greater neurotoxicity. *Solid line* TJ-107, *broken line* Placebo

The time to occurrence of grade 2 or greater OPN is shown in Fig. 2. In patients who developed grade 2 or greater OPN, the median time to occurrence was 5.5 months (95 %CI 4.1–N.A.) in the TJ-107 group and 3.9 months (95 % CI 2.3–6.4) in the placebo group (RR 0.65; 95 % CI 0.36–1.17). The median time to occurrence of grade 3 neurotoxicity was better controlled in the TJ-107 group (RR 0.71; 95 % CI 0.29–1.77). The median frequency of occurrence of OPN at 26 weeks was 54.1 and 62.5 % (RR 0.86) in the TJ-107 and placebo groups, respectively.

When we stratified the patients based on FOLFOX regimen (i.e., FOLFOX4 vs. mFOLFOX6) and performed a subanalysis to determine whether there was a difference in the effects of TJ-107 on the occurrence of OPN, we found that there was no significant difference between

Table 3 Median FACT/GOG-Ntx-12 score

	TJ-107 ($N = 44$)	Placebo ($N = 45$)	P value
8 weeks	6.0	9.0	0.421
26 weeks	7.0	10.5	0.151

* FACT/GOG-Ntx-12: Functional Assessment of Cancer Therapy/Gynecological Oncology Group-Neurotoxicity-12 score

Table 4 Tumor response rate

Overall	TJ-107 ($N = 27$)	Placebo ($N = 23$)	P value
Complete response (CR)	1	1	
Partial response (PR)	14	10	
Stable disease (SD)	9	11	
Progression disease (PD)	3	1	
Not evaluable (NE)	0	0	
CP + PR	15 (56 %)	11 (48 %)	0.777
95 % CI	0.37–0.74	0.27–0.68	
CR + PR + SD	24 (89 %)	22 (96 %)	0.614
95 % CI	0.77–1.00	0.87–1.00	

treatment groups albeit the small sample size in each group.

The median FACT scores of the TJ-107 and placebo groups were 6.0 vs. 9.0 ($P = 0.421$) at 8 weeks and 7.0 vs. 10.5 ($P = 0.151$) at 26 weeks (Table 3). Although the differences were statistically unremarkable, patients receiving TJ-107 tended to show milder symptoms of neurotoxicity than those who received placebo.

Tumor response rate

The anti-tumor effect was assessed in 27 (TJ-107) and 23 (placebo) patients who had a target lesion at the time of enrollment. Bevacizumab was administered in 74 % (20/27) and 74 % (17/23) of patients in the TJ-107 group and the placebo group, respectively (Table 4).

The overall chemotherapy response rates were 56 % in the TJ-107 group and 48 % in the placebo group. In addition, 89 % (TJ-107) and 96 % (placebo) of patients demonstrated disease control (complete response, partial response, or stable disease) (Table 4).

Toxicity assessment

TJ-107 used in this study appeared to be well tolerated. There were no significant differences between the two groups in terms of toxicity. The most common adverse events likely caused by the chemotherapy were anorexia, fatigue, nausea, and stomatitis, which were reported at similar rates from patients of both groups (Table 5). Vomiting was significantly suppressed in patients on TJ-107 compared with controls (9 vs. 29 %, $P = 0.029$). In the context of systemic chemotherapy, most of these events were likely related to chemotherapy-induced toxicity, yet none of them were considered TJ-107 related. Eighteen hematologic toxicity events of grade 3 or greater (15 neutropenia) in the placebo group were reported, and 12 events (10 neutropenia) were noted in the TJ-107 group (Table 6). One patient in the placebo group died as a direct result of progressive disease.

Table 5 Incidence of adverse events

All grades	TJ-107 ($N = 44$) (%)	Placebo ($N = 45$) (%)	P value
Fatigue	25 (57)	26 (58)	1.000
Anorexia	27 (61)	22 (49)	0.289
Nausea	20 (45)	28 (62)	0.139
Vomiting	4 (9)	13 (29)	0.029
Stomatitis	19 (43)	16 (36)	0.519
Diarrhea	15 (34)	10 (22)	0.245
Hand-food syndrome	11 (25)	7 (16)	0.302
Allergic reaction	8 (18)	4 (9)	0.230
Febrile neutropenia	0 (0)	2 (4)	0.494
Constipation	2 (5)	2 (4)	1.000
Ileus	0 (0)	2 (4)	0.494
Total Bilirubin	4 (9)	4 (9)	1.000
AST	13 (30)	23 (51)	0.052
ALT	10 (23)	19 (42)	0.070
ALP	13(30)	19(42)	0.271

Table 6 Incidence of hematologic toxicity events

	TJ-107 ($N = 44$) (%)	Placebo ($N = 45$) (%)	P value
All grades			
Leukopenia	21 (48)	27 (60)	0.291
Neutropenia	15 (34)	21 (47)	0.282
Anemia	30 (68)	31 (69)	1.000
Thrombocytopenia	12 (27)	15 (33)	0.646
Grade ≥ 3			
Leukopenia	1 (2)	2 (4)	1.000
Neutropenia	10 (23)	15 (33)	0.347
Anemia	1 (2)	1 (2)	1.000
Thrombocytopenia	0 (0)	0 (0)	1.000

Discussion

This is the first placebo-controlled, randomized, exploratory study that assessed the efficacy of oral TJ-107 in the treatment of OPN in colorectal cancer patients undergoing oxaliplatin-based chemotherapy.

Our randomized, phase 2, exploratory trial using a placebo was designed to assess the potential success of oral TJ-107 in the phase 3 setting, rather than provide solid data on its efficacy. Results of this study showed promising relative risk that support the clinical activity of oral TJ-107 against OPN, particularly acute cold-associated neuropathy, in patients who received FOLFOX therapy (FOLFOX4 or mFOLFOX6) for colorectal cancer without imposing negative impact on oxaliplatin-based anti-tumor effect. Additionally, TJ-107 did not cause any adverse effects during the trial. Our findings, which showed improvement in both CTCAE grades and patient-rated FACT/GOG-Ntx scores, suggest that TJ-107 delays the occurrence of grade 2 or greater OPN during active treatment although its therapeutic effect may plateau after 6.5 months of continuous administration and that the development of neurotoxicity was not correlated with the completion of oxaliplatin treatment. Given the difficulty of generating statistically robust data with a small sample size, we surmised that our data warrant further investigation in a large phase 3 setting.

As an exploratory, phase 2 trial of patients with advanced or relapsed colorectal cancer (some with unresectable cancer), we conducted the endpoint assessment after 8 cycles rather than at treatment completion on the basis of a previous study that reported the high likelihood of detecting the side effects of oxaliplatin after 8 cycles [19], suggesting that this time point may be critical for deciding whether to continue oxaliplatin-based chemotherapy. Furthermore, a postmarketing drug surveillance of TJ-107 in Japan has shown that the median time to occurrence of grade 3 neuropathy with motor disorder was after 8 cycles. Taken together, these data suggest the evaluation of neuropathy at its peak incidence after 8 cycles to be clinically more meaningful than delaying the evaluation until treatment completion.

TJ-107 is a complex drug containing 10 medicinal herbs with a wide spectrum of pharmacologic actions [16]. Experimental studies have shown that TJ-107 relieves neurologic symptoms of diabetic peripheral neuropathy such as cold hyperalgesia and mechanical allodynia [13–15] primarily by the action of its analgesic component, detoxified Aconiti Tuber. The purported mechanisms by which this component works in concert with the other components of TJ-107 to exert a neuroprotective effect include (1) evoking the release of dynorphin and activating endogenous κ-opioid receptors to improve numbness or paresthesia [20, 21], (2) decreasing the release of transmitter proteins and sensory receptors associated with C-fiber nociceptor activation [22, 23], and (3) promoting nitric oxide production to improve blood supply to the nerves [24]. Furthermore, a recent experimental study has demonstrated that TJ-107 ameliorates the pain associated with OPN in rats without affecting the anti-tumor activity of oxaliplatin [25], which is in line with our findings. Interestingly, we also found that TJ-107 significantly decreased vomiting compared with placebo. The precise mechanism remains unclear but one of the components of TJ-107, Poria (*Poria cocos* Wolf), has shown an antiemetic effect through 5-HT3A receptor inhibition [26, 27].

According to the Multicenter International Study of Oxaliplatin, 5-Fluorouracil and Leucovorin in the Adjuvant Treatment of Colon Cancer (MOSAIC) study, the reported incidences of OPN were as follows: grade 1 (48 %), grade 2 (32 %), and grade 3 (12 %) [1]. In the present study, the incidence of grade 2 and grade 3 OPN in the placebo group until the 8th cycle was 51 % and 13 %, respectively, which is consistent with the MOSAIC study [1]. There was no marked difference in time to treatment failure in this study. One possible explanation for this is that even if greater than grade 2 OPN had occurred once, oxaliplatin administration was continued so long as OPN was downgraded to grade 2 on the day of administration. Another possibility is that patients may not acknowledge or report neuropathic symptoms for fear of missing out on an effective cancer treatment. Thus, it seems imperative to discover an agent that has sufficient evidence to decrease OPN development.

Many agents have been tested, in both humans and experimental animals, to ameliorate OPN [28]. Recently, the antidepressant drug venlafaxine, which is also used to manage pain associated with diabetic peripheral neuropathy, has been reported to significantly decrease the incidence of acute OPN in a placebo-controlled, randomized, phase 3 trial; however, grade 1–2 vomiting was observed more frequently in patients who received venlafaxine [29]. TJ-107 has also been used to treat painful diabetic peripheral neuropathy [13–15], but our study showed that TJ-107 significantly decreased vomiting compared to placebo, and other common adverse events due to chemotherapy did not worsen with TJ-107 treatment. Effective preventive treatments must not only mitigate neurotoxicity but must also preserve the antineoplastic effect of chemotherapeutic drugs. In this study, no between-group differences were found in response rates to chemotherapy or in the survival rates, suggesting that TJ-107 had no influence on FOLFOX therapy. Moreover, TJ-107 is an easily administered alternative that does not produce serious adverse effect, rendering it conducive to increasing compliance among patients and health care practitioners in a cancer treatment setting.

This is the first, randomized, phase 2, exploratory trial of TJ-107 whose study design itself is comparable to that

of an older phase 3 trial design. The primary objective of this phase 2 trial study was to determine whether our findings would warrant validation in a phase 3 setting and not necessarily to obtain concrete data that show statistical significance. In other words, our aim was to define the characteristics of TJ-107 against OPN relative to placebo in order to refine the design of a phase 3 trial. Through this study, we were able to obtain a more accurate estimation of sample size and confirm that TJ-107 was similar to placebo in terms of toxicity despite the small sample size, and TJ-107 prevented the progression and development of severe neurotoxicity, one of the primary dose-limiting factors of oxaliplatin-based chemotherapy. Taken together, our findings suggest that this trial served as an effective platform for testing the efficacy of a novel agent like TJ-107 in oncology and for designing and accelerating the transition from phase 2 to a large phase 3 trial that employs objective measures.

Conclusions

Findings from this phase 2, exploratory trial suggest that oral TJ-107 has acceptable margins of safety and tolerability and a promising effect in delaying the onset of grade 2 or greater OPN in colorectal cancer patients treated with oxaliplatin.

Acknowledgments The authors thank the patients and all investigators and research support staff at the participating centers. We would also like to thank the trial management group, independent data monitoring and trial steering committees for overseeing the trial. We also thank Chigusa Abe for her excellent work as the principle research coordinator. Funding was partially provided by Epidemiological and Clinical Research Information Network (ECRIN). ECRIN provided peer-reviewed approval for the trial but had no other role in study design, collection, analysis, interpretation of data, or writing of the report.

Conflict of interest None.

References

1. André T, Boni C, Mounedji-Boudiaf L, Navarro M, Tabernero J, Hickish T, Topham C, Zaninelli M, Clingan P, Bridgewater J, Tabah-Fisch I, de Gramont A (2004) Multicenter international study of oxaliplatin/5-fluorouracil/leucovorin in the adjuvant treatment of colon cancer (MOSAIC) Investigators: Oxaliplatin, fluorouracil, and leucovorin as adjuvant treatment for colon cancer. N Engl J Med 350:2343–2351
2. Lucchetta M, Lonardi S, Bergamo F, Alberti P, Velasco R, Argyriou AA, Briani C, Bruna J, Cazzaniga M, Cortinovis D, Cavaletti G, Kalofonos HP (2012) Incidence of atypical acute nerve hyperexcitability symptoms in oxaliplatin-treated patients with colorectal cancer. Cancer Chemo Pharm 70:899–902
3. Cersosimo RJ (2005) Oxaliplatin-associated neuropathy: a review. Ann Pharmacother 39:128–135
4. de Gramont A, Figer A, Seymour M, Homerin M, Hmissi A, Cassidy J, Boni C, Cortes-Funes H, Cervantes A, Freyer G, Papamichael D, Le Bail N, Louvet C, Hendler D, de Braud F, Wilson C, Morvan F, Bonetti A (2000) Leucovorin and fluorouracil with or without oxaliplatin as first-line treatment in advanced colorectal cancer. J Clin Oncol 18:2938–2947
5. Krishnan AV, Goldstein D, Friedlander M, Kiernan MC (2005) Oxaliplatin-induced neurotoxicity and the development of neuropathy. Muscle Nerve 32:51–60
6. Land SR, Kopec JA, Cecchini RS, Ganz PA, Wieand HS, Colangelo LH, Murphy K, Kuebler JP, Seay TE, Needles BM, Bearden JD 3rd, Colman LK, Lanier KS, Pajon ER Jr, Cella D, Smith RE, O'Connell MJ, Costantino JP, Wolmark N (2007) Neurotoxicity from oxaliplatin combined with weekly bolus fluorouracil and leucovorin as surgical adjuvant chemotherapy for stage II and III colon cancer: NSABP C-07. J Clin Oncol 25:2205–2211
7. Leonard GR, Wright MA, Quinn MG, Fioravanti S, Harold N, Schuler B, Thoomas RR, Grem JL (2005) Survey of oxaliplatin-associated neurotoxicity using an interview-based questionnaire in patients with metastatic colorectal cancer. BMC Cancer 5:116–126
8. Kaley TJ, Deangelis LM (2009) Therapy of chemotherapy-induced peripheral neuropathy. Br J Haematol 145:3–14
9. Cavaletti G, Alberti P, Marmiroli P (2011) Chemotherapy-induced peripheral neurotoxicity in the era of pharmacogenomics. Lancet Oncol 12:1151–1161
10. Wu Z, Ouyang J, He Z, Zhang S (2012) Infusion of calcium and magnesium for oxaliplatin-induced sensory neurotoxicity in colorectal cancer: a systematic review and meta-analysis. Eur J Cancer 48:1791–1798
11. Cavaletti G, Frigeni B, Lanzani F, Mattavelli L, Susani E, Alberti P, Cortinovis D, Bidoli P (2010) Chemotherapy-induced peripheral neurotoxicity assessment: a critical revision of the currently available tools. Eur J Cancer 46:479–494
12. Kono T, Kanematsu T, Kitajima M (2009) Exodus of Kampo, traditional Japanese medicine, from the complementary and alternative medicines: is it time yet? Surgery 146:837–840
13. Nagaki Y, Hayasaka S, Hayasaka Y, Kadoi C, Sekiya N, Terasawa K, Sakakibara I (2003) Effects of goshajinkigan on corneal sensitivity, superficial punctate keratopathy and tear secretion in patients with insulin-dependent diabetes mellitus. Am J Chin Med 31:103–109
14. Tawata M, Kurihara A, Nitta K, Iwase E, Gan N, Onaya T (1994) The effects of goshajinkigan, a herbal medicine, on subjective symptoms and vibratory threshold in patients with diabetic neuropathy. Diabetes Res Clin Pract 26:121–128
15. Uno T, Ohsawa I, Tokudome M, Sato Y (2005) Effects of Goshajinkigan on insulin resistance in patients with type 2 diabetes. Diabetes Res Clin Pract 69:129–135
16. Kono T, Mamiya N, Chisato N, Ebisawa Y, Yamazaki H, Watari J, Yamamoto Y, Suzuki S, Asama T, Kamiya K (2009) Efficacy of Goshajinkigan for peripheral neurotoxicity of oxaliplatin in patients with advanced or recurrent colorectal cancer. Evid Based Complement Alternat Med. doi:10.1093/ecam/nep200
17. Nishioka M, Shimada M, Kurita N, Iwata T, Morimoto S, Yoshikawa K, Higashijima J, Miyatani T, Kono T (2011) The Kampo medicine, Goshajinkigan, prevents neuropathy in patients treated by FOLFOX regimen. Int J Clin Oncol 16:322–327
18. Kono T, Mishima H, Shimada M, Morita S, Sakamoto J (2009) GONE Investigators: preventive effect of goshajinkigan on peripheral neurotoxicity of FOLFOX therapy: a placebo-controlled double-blind randomized phase II study (the GONE Study). Jpn J Clin Oncol 39:847–849

19. Haller DG (2000) Safety of oxaliplatin in the treatment of colorectal cancer. Oncology (Williston Park) 12(Suppl 11):15–20
20. Omiya Y, Goto K, Suzuki Y, Ishige A, Komatsu Y (1999) Analgesia-producing mechanism of processed Aconiti tuber: role of dynorphin, an endogenous kappa-opioid ligand, in the rodent spinal cord. Jpn J Pharmacol 79:295–301
21. Gotoh A, Goto K, Sengoku A, Shirakawa T, Akao Y, Fujisawa M, Okada H, Arakawa S, Kamidono S (2004) Inhibition mechanism of Gosha-jinki-gan on the micturition reflex in rats. J Pharm Sci 96:115–123
22. Imamura T, Ishizuka O, Aizawa N, Zhong C, Ogawa T, Nakayama T, Tanabe T, Nishizawa O (2008) Gosha-jinki-gan reduces transmitter proteins and sensory receptors associated with C fiber activation induced by acetic acid in rat urinary bladder. Neurourol Urodyn 27:832–837
23. Joseph EK, Chen X, Bogen O, Levine JD (2008) Oxaliplatin acts on IB4-positive nociceptors to induce an oxidative stress-dependent acute painful peripheral neuropathy. J Pain 9:463–472
24. Hu X, Sato J, Oshida Y, Xu M, Bajotto G, Sato Y (2003) Effect of Gosha-jinki-gan (Chinese herbal medicine: Niu-Che-Sen-Qi-Wan) on insulin resistance in streptozotocin-induced diabetic rats. Diabetes Res Clin Pract 59:103–111
25. Ushio S, Egashira N, Sada H, Kawashiri T, Shirahama M, Masuguchi K, Oishi R (2012) Goshajinkigan reduces oxaliplatin-induced peripheral neuropathy without affecting anti-tumour efficacy in rodents. Eur J Cancer 48:1407–1413
26. Tai T, Akita Y, Kinoshita K, Koyama K, Takahashi K, Watanabe K (1995) Anti-emetic principles of Poria cocos. Planta Med 61:527–530
27. Lee JH, Lee YJ, Kang SW, Kim Y, Shin M, Hong M, Seo EK, Kim SH, Nah SY, Bae H (2010) Effects of protostane-type triterpenoids on the 5-HT3A receptor-mediated ion current in Xenopus oocytes. Brain Res 1331:20–27
28. Cavaletti G, Marmiroli P (2010) Chemotherapy-induced peripheral neurotoxicity. Nat Rev Neurol 6:657–666
29. Durand JP, Deplanque G, Montheil V, Gornet JM, Scotte F, Mir O, Cessot A, Coriat R, Raymond E, Mitry E, Herait P, Yataghene Y, Goldwasser F (2012) Efficacy of venlafaxine for the prevention and relief of oxaliplatin-induced acute neurotoxicity: results of EFFOX, a randomized, double-blind, placebo-controlled phase III trial. Ann Oncol 23:200–205

DOI:10.1093/jnci/djt337 JNCI Journal of the National Cancer Institute Advance Access published October 9, 2013

REVIEW

Disease-Free Survival as a Surrogate for Overall Survival in Adjuvant Trials of Gastric Cancer: A Meta-Analysis

Koji Oba, Xavier Paoletti, Steven Alberts, Yung-Jue Bang, Jacqueline Benedetti, Harry Bleiberg, Paul Catalano, Florian Lordick, Stefan Michiels, Satoshi Morita, Yasuo Ohashi, Jean-pierre Pignon, Philippe Rougier, Mitsuru Sasako, Junichi Sakamoto, Daniel Sargent, Kohei Shitara, Eric Van Cutsem, Marc Buyse, Tomasz Burzykowski; on behalf of the GASTRIC group

Manuscript received February 12, 2013; revised July 25, 2013; accepted July 25, 2013.

Correspondence to: Koji Oba, PhD, Translational Research and Clinical Trial Center, Hokkaido University Hospital, Kita 14, Nishi 5, Kita-ku, Sapporo, Hokkaido 0608648, Japan (e-mail: k oba@huhp hokudai.ac.jp).

Background In investigations of the effectiveness of surgery and adjuvant chemotherapy for gastric cancers, overall survival (OS) is considered the gold standard endpoint. However, the disadvantage of using OS as the endpoint is that it requires an extended follow-up period. We sought to investigate whether disease-free survival (DFS) is a valid surrogate for OS in trials of adjuvant chemotherapy for gastric cancer.

Methods The GASTRIC group initiated a meta-analysis of individual patient data collected in randomized clinical trials comparing adjuvant chemotherapy vs surgery alone for patients with curatively resected gastric cancer. Surrogacy of DFS was assessed through the correlation between the endpoints as well as through the correlation between the treatment effects on the endpoints. External validation of the prediction based on DFS was also evaluated.

Results Individual patient data from 14 randomized clinical trials that included a total of 3288 patients were analyzed. The rank correlation coefficient between DFS and OS was 0.974 (95% confidence interval [CI] = 0.971 to 0.976). The coefficient of determination between the treatment effects on DFS and on OS was as high as 0.964 (95% CI = 0.926 to 1.000), and the surrogate threshold effect based on adjusted regression analysis was 0.92. In external validation, the six hazard ratios for OS predicted according to DFS were in very good agreement with those actually observed for OS.

Conclusions DFS is an acceptable surrogate for OS in trials of cytotoxic agents for gastric cancer in the adjuvant setting.

J Natl Cancer Inst

Gastric cancer is the fourth most common malignancy in the world, affecting 989 000 patients in 2008 (7.8% of all cancers) (1). The most effective treatment for localized disease is surgery, but even after curative resection, recurrence is noted in more than half the cases of advanced-stage disease. This poor outcome has prompted major efforts to explore different adjuvant therapies. However, over the last three decades, despite some successful large-scale trials (2–5), only modest improvement has been achieved in survival. Our group recently reported the results of a meta-analysis of individual data that showed a lower risk of death with postoperative adjuvant chemotherapy than with surgery alone (overall hazard ratio [HR] =0.82; $P < .0001$) (6). However, the efficacy of adjuvant chemotherapy is still far from satisfactory, and further investigation into more effective treatments for patients with resectable gastric cancer is warranted.

Historically, the 5-year overall survival (OS) rate has typically been the most quoted metric for judging the success of a particular treatment. This endpoint has the advantage of being simple to measure, easy to interpret, and clinically meaningful. However, the main disadvantages of this endpoint are that it requires an extended follow-up period and its measurement is potentially diluted by nonmalignant causes of death and therapies for recurrent/advanced disease.

A reasonable candidate for a surrogate of OS in the adjuvant setting is disease-free survival (DFS), which is defined here as the time to cancer recurrence, second cancer, or death from any cause. Recent meta-analyses have been used to validate DFS as a surrogate for OS in other tumor types (7,8). If DFS could replace OS in the assessment of the efficacy of new treatments in clinical trials testing adjuvant treatment for patients with curatively resected gastric cancer, the trial duration and costs would be reduced. We performed a comprehensive meta-analysis of data from 3838 individual patients randomized in 17 trials on curatively resected gastric cancer; documented DFS values, which were available for 3371 of the patients from 14 trials, were used to evaluate DFS as a surrogate endpoint for OS.

Methods

Study Selection

Our analyses were based on a meta-analysis of individual patient data (IPD) described in detail elsewhere (6). IPD from all randomized trials comparing adjuvant chemotherapy with surgery alone for resectable gastric cancers were sought electronically from MEDLINE, the Cochrane Central Register of Controlled Trials,